Marine Natural Products

Zitierweise: *Angew. Chem. Int. Ed.* **2023,** *62,* e202218085
Internationale Ausgabe: doi.org/10.1002/anie.202218085
Deutsche Ausgabe: doi.org/10.1002/ange.202218085

Somalactams A–D: Anti-inflammatory Macrolide Lactams with Unique Ring Systems from an Arctic Actinomycete Strain

Fan Yang[+], Moli Sang[+], Jing-Rong Lu, Hui-Min Zhao, Yike Zou, Wei Wu, Yong Yu, Ya-Wei Liu, Wencheng Ma, Yun Zhang, Wei Zhang, and Hou-Wen Lin**

In memory of Yi-Zhen Yan

Abstract: Four new PKS-NRPS-derived macrolide lactams with three unique ring fusion types were discovered from the Arctic sponge associated actinomycete *Streptomyces somaliensis* 1107 using a genome mining strategy. Their structures were elucidated by a combination of MS, NMR spectroscopic analysis, and single-crystal X-ray diffraction. Biosynthetically, a novel gene cluster *sml* consisting of three polyketide synthases and one hybrid polyketide synthase-nonribosomal peptide synthetase together with cytochrome P450s and flavin-containing monooxygenases and oxidoreductases was demonstrated to assemble the unique skeleton. Pharmacological studies revealed that compound **1** displayed a potent anti-inflammatory effect without cytotoxicity. It inhibited IL-6 and TNF-α release in the serum of LPS-stimulated RAW264.7 macrophage cells with IC_{50} values of 5.76 and 0.18 μM, respectively, and modulated the MAPK pathway. Moreover, compound **1** alleviated LPS-induced systemic inflammation in our transgenic fluorescent zebrafish model.

Introduction

Polar microorganisms are precious resources. Microorganisms adapt to extreme environments and produce structurally intriguing secondary metabolites; for example, cold-water marine natural products are valuable, promising sources for pharmaceutical research and development.[1] In particular, *Streptomyces* actinomycetes existing under such conditions are precious mines for structurally diverse bioactive secondary metabolites, such as pyrrolosesquiterpenes,[2] bisindole alkaloids,[3] polyketide macrolactams,[4] and benzoxazoles.[5]

As part of our search for new anti-inflammatory molecules from marine animals and microbes during an Arctic Ocean research expedition, a strain *S. somaliensis* 1107 (Figures S1 and S2 in the Supporting Information) was isolated from an Arctic *Haliclona* sponge. This strain is of particular interest owing to its potential anti-inflammatory activity in our established screening model (Figure S3).[6] Secondly, genome mining of this strain by online antiSMASH[7] identified 16 putative biosynthetic gene clusters (BGCs) for secondary metabolite biosynthesis. Of special interest, one conspicuous cluster *sml* is organized with three polyketide synthase (PKS) and one polyketide synthase-nonribosomal peptide synthetase (PKS-NRPS) encoding genes in a PKS-NRPS-PKS pattern. The cluster contained 26 open reading frames (ORFs) spanning 75.8 kb and co-clustered with a number of P450s, flavin-containing monooxygenases, oxidoreductases, and potential regulator encoding genes (Table S1).

Detailed analysis of these four megasynthases revealed that the PKS-NRPS hybrid BGC *sml* consists of 40 domains within 9 modules (Table S1), which perfectly matched the typical type I polyketide rules and NRPS pattern of collinearity.[8,9] Thus, it is reasonable to predict that natural products assembled by this gene cluster would be macrolide

[*] Dr. F. Yang,[+] J.-R. Lu, H.-M. Zhao, Dr. W. Wu, Y.-W. Liu, Prof. Dr. H.-W. Lin
Department of Pharmacy, Research Center for Marine Drugs, Renji Hospital School of Medicine, State Key Laboratory of Microbial Metabolism, Shanghai Jiao Tong University
Shanghai 200127 (China)
E-mail: franklin67@126.com

M. Sang,[+] W. Ma, Prof. Dr. W. Zhang
State Key Laboratory of Microbial Technology, Shandong University, Qingdao, Shandong 266237
and
Shenzhen Research Institute of Shandong University
Shenzhen 518057 (China)
E-mail: zhang_wei@sdu.edu.cn

Dr. Y. Zou
Department of Chemistry and Biochemistry, University of California Los Angeles, CA 90095-1569 (USA)

Dr. Y. Yu
Key Laboratory of Polar Science, Ministry of Natural Resources; Antarctic Great Wall Ecology National Observation and Research Station; Polar Research Institute of China, Shanghai, 200136, China
and
School of Oceanography (SOO), Shanghai Jiao Tong University
Shanghai 200030 (China)

Y. Zhang
Biology Institute, Qilu University of Technology (Shandong Academy of Sciences)
Jinan 250103 (China)

[+] These authors contributed equally to this work.

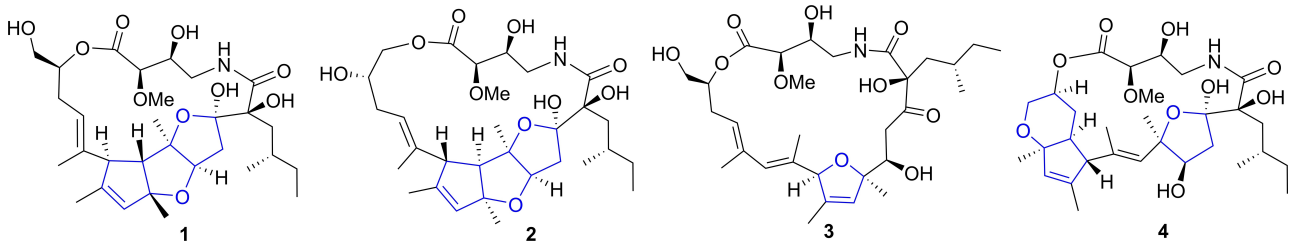

Figure 1. Chemical structures of compounds **1**–**4**.

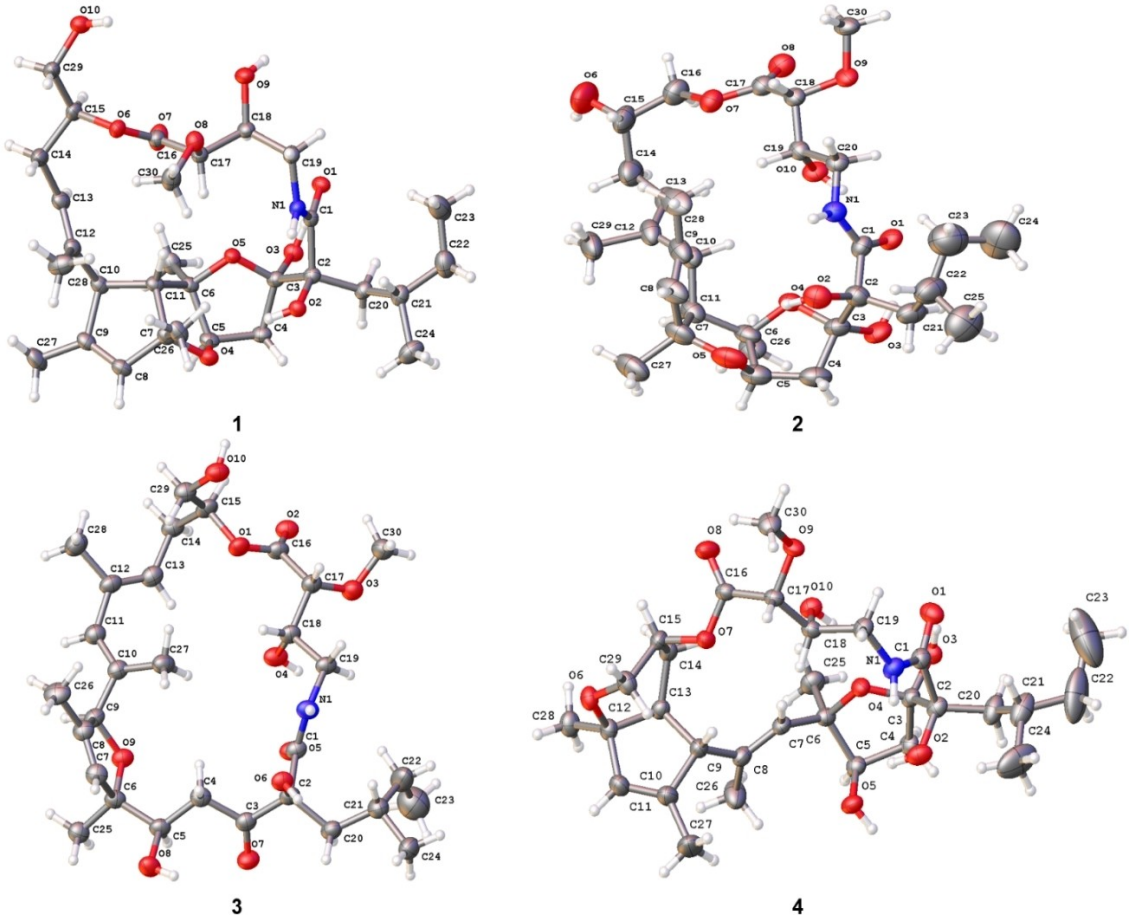

Figure 2. X-ray crystal structures of compounds **1**–**4**.

lactams with highly modified structures. In particular, SmlB-D comprised two modules, while three modules were found with the hybrid PKS-NRPS SmlA terminated with a thioesterase (TE) domain. The first domain of SmlB was predicted as an acyl carrier protein (ACP), while the other three megasynthases were initiated by a ketosynthase (KS) domain, suggesting a stand-alone acyltransferase (*trans*-AT) may act *in trans* to load the initial substrate.[9] Alternatively, two continuous AT domains were found within the architecture of module 1 in SmlB, and the first AT domain (AT1) may act as the loading domain.

To decipher the natural products assembled by the unique gene cluster *sml* of *S. somaliensis* 1107, we performed an OSMAC (one strain many compounds) investigation,[10] which led to the detection and isolation of somalactams A–D (**1**–**4**) from ISP2 medium. In-frame deletion by CRISPR-Cas9 demonstrated that the *sml* gene cluster is responsible for the biosynthesis of somalactams. Further, pharmacological studies revealed that somalactam A (**1**) displayed an anti-inflammatory effect without cytotoxicity.

Results and Discussion

When *S. somaliensis* 1107 was cultured in ISP2 medium for 7 days, a series of peaks with a molecular ion peak at *m/z*

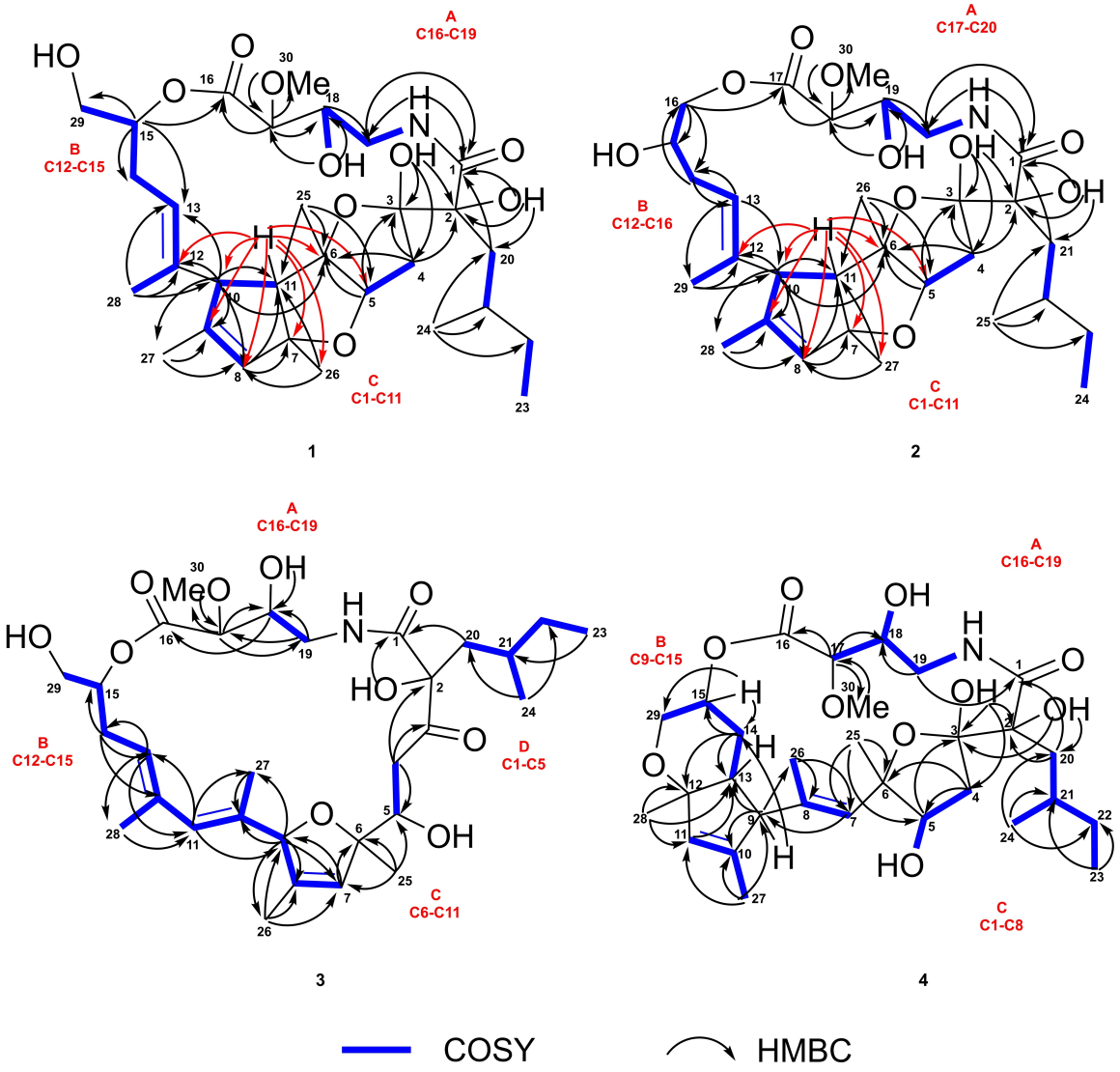

Figure 3. The key 2D NMR correlations of compounds **1–4**.

604 were detected by LC–MS analysis (Tables S2 and S3, Figure S4). Subsequently, the deletion of PKS SmlD by a CRISPR-Cas9 mediated in-frame deletion strategy[11] abolished the production of these targeted peaks together with the anti-inflammatory activity (Figure S5). Further, the in-frame deletion of a putative P450 encoding gene *sml5* also led to the disappearance of peaks at *m/z* 604, while three new peaks were observed with a molecular ion peak at *m/z* 588 (Figure S5). Together, these results demonstrated that the novel PKS-NRPS-PKS gene cluster *sml* is responsible for producing the anti-inflammatory metabolites.

Through chemical investigation of *S. somaliensis* 1107, four new macrolide lactams **1–4** were isolated and named somalactams A–D, respectively (Figure 1). Interestingly, somalactam A (**1**) and somalactam B (**2**) possess a unique hexahydro-2*H*-cyclopenta[*b*]furo[2,3-*d*]furan ring system with hemiacetal functionality.

Somalactam A (**1**) was obtained as a white amorphous solid. Its molecular formula was determined to be $C_{30}H_{47}NO_{10}$ from the HRESIMS pseudomolecular ion peak at *m/z* 604.3099 $[M+Na]^+$ ($C_{30}H_{47}NO_{10}Na$, *calcd.* 604.3098), indicating eight double-bond equivalents. The IR absorptions at 1732 and 1643 cm^{-1} suggested that **1** contained amide and ester groups. The ^1H NMR spectrum displayed the characteristic signals of six methyl groups at $\delta_H = 0.76$ (t, $J = 7.4$ Hz, H_3-23), 0.90 (d, $J = 6.8$ Hz, H_3-24), 1.27 (s, H_3-25), 1.50 (s, H_3-26), 1.56 (s, H_3-27), and 1.40 ppm (s, H_3-28); one methoxy group at $\delta_H = 3.46$ ppm (s, H_3-30); and two olefinic hydrogen atoms at $\delta_H = 5.24$ (s, H-8) and 5.18 ppm (dd, $J =$ 9.5, 3.0 Hz, H-13). The ^{13}C NMR and DEPT spectra showed that **1** had 30 carbon atoms, including 8 non-protonated carbon atoms, 9 methines, 6 methylenes, and 7 methyl groups (Table S5).

The COSY and HMBC spectra of **1** suggested that it comprised three fragments A–C (Figure S7). For fragment A (C16-C19), the methoxy and hydroxy groups were located at C17 and C18, respectively, as indicated by the COSY correlations of 18-OH/H-18/H-19b/NH and the HMBC

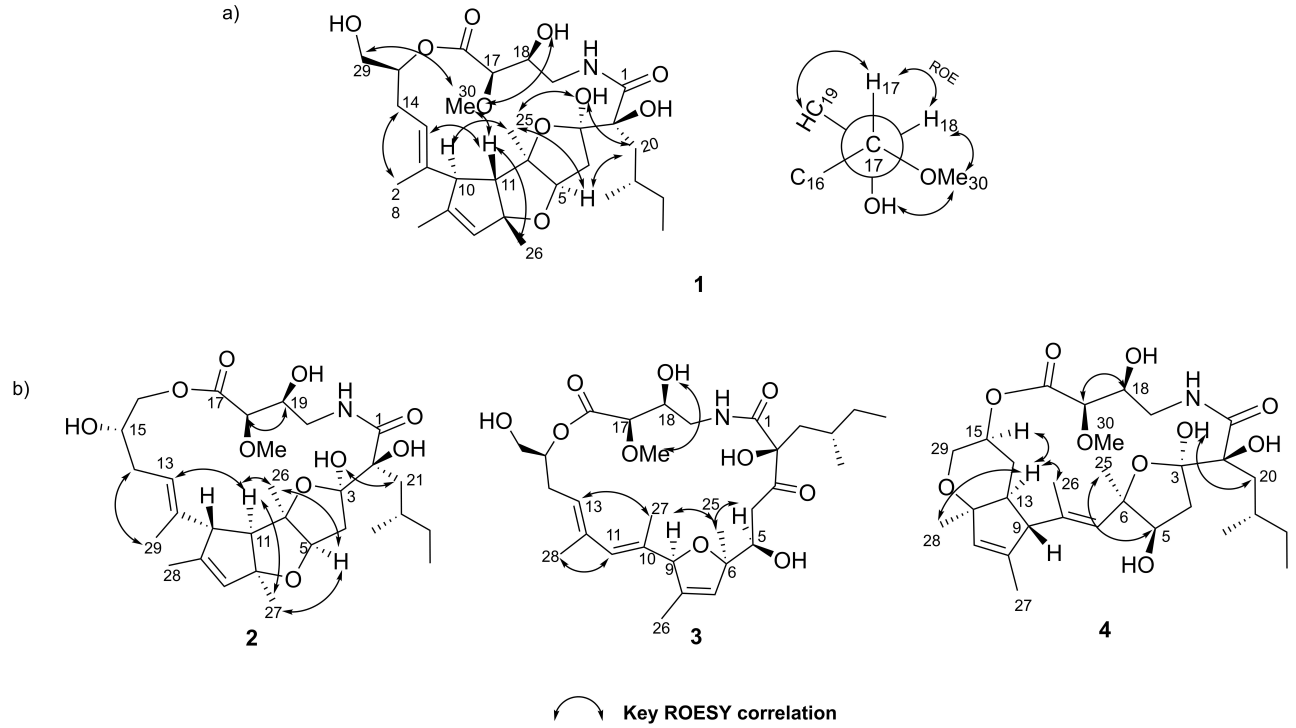

Figure 4. a) Relative configuration analysis of compound **1** and rotamers determined for C-17-C-18; b) Relative configuration analysis of compounds **2**–**4**.

correlations from the oxymethine proton H-17 to C30, C18, and the ester carbonyl C16 ($\delta_C = 171.1$ ppm); from H-18 to C17 and C19; and from 30-OMe and the exchangeable proton 18-OH ($\delta_H = 4.62$ ppm) to C17. The HMBC correlations from the methyl H_3-28 to the olefin carbon atoms C12 and C13, and the COSY correlations of H_3-28/H-13 and H-13/H_2-14/H-15/H_2-29, suggested the existence of fragment B (C12-C15), which was connected to fragment A through an ester group as confirmed by the HMBC correlations from H-15 to C16, C14, and C13. In fragment C (C1-C11), a tetrahydrofuran moiety was assigned on the basis of the HMBC correlations from H-4b to the oxygenated quaternary carbon C3 ($\delta_C = 109.9$ ppm), from H-4a to two other oxygenated quaternary carbon atoms C2 ($\delta_C = 78.3$ ppm) and C6 ($\delta_C = 94.9$ ppm), and from the oxymethine hydrogen atom H-5 to C3 and C6, as well as the COSY correlation of H-4a/H-5. The HMBC correlations from 2-OH ($\delta_H =$ 4.12 ppm) to C1, C2, and C20 and from 3-OH ($\delta_H =$ 6.09 ppm) to C2, C3, and C4 placed the two hydroxy groups at C2 and C3, respectively. The COSY cross-peaks of H-8/H-10 and H-10/H-11, together with the HMBC correlations from H_3-27 to C8, C9, and C10 and from H_3-26 to C7, C8, and C11, illustrated the existence of a five-membered ring system (C7-C11). C11 was connected to C6 as confirmed by the HMBC correlations from H_3-25 to C5, C6, and C11 and from H-10/H-11 to C6. The ether linkage between C5 and C7 was established by the characteristic chemical shifts of C5 ($\delta_C = 84.7$ ppm) and C7 ($\delta_C = 96.0$ ppm) and the degree of unsaturation calculated from the molecular formula. Therefore, an unprecedented hexahydro-2*H*-cyclopenta[*b*]furo [2,3-*d*]furan ring system containing hemiacetal functionality was found in fragment C of **1**, which was further proven by the key HMBC correlations from H-11 to C6, C7, C8, C9, C10, C12, and C26 (red arrows in Figure 3). The HMBC correlations from H_3-28 to C10, C12, and C13 and from NH/H-19a/H-20a to the amide carbonyl C1 atom suggested the connection of the three fragments, thus completing the planar structure of **1**.

A combination of homo-($^3J_{H,H}$) and heteronuclear ($^2J_{C,H}$) coupling-constant-based configurational analyses, alongside extensive ROE evidence (in DMSO-d_6 and $CDCl_3$) and ROE irradiation experiments, were used to determine the relative configuration within the macrolide lactam core of **1**. Figure 4a shows the extensive NMR analyses of the C17-C18 segment of **1**. The ROESY correlations of H-18/H-17, H-18/30-OMe, H-17/H-19b, and 18-OH/30-OMe, together with small ^3J (H-17 (br.s), H-18), small ^2J (H-17, C18, acquired by HETLOC), and large ^2J (C17, H-18, 9.8 Hz acquired by HETLOC) coupling constants, suggested the rotamer pattern as depicted according to a previously reported *J*-based configuration analysis method.[12] The ROESY correlation between H_2-29 and 30-OMe indicated that they were cofacial; a ROE irradiation experiment was also carried out for confirmation owing to their adjacent ^{1}H NMR chemical shifts (Figure S35). The *E* configuration of the Δ^{12} double bond was established using the ROESY correlation of H_3-28/H-14a. The diagnostic ROESY correlations of H-10/H_3-25, H-5/H_3-25, H-5/H-20a, 3-OH/H-20a, and H_3-25/3-OH suggested that they were oriented on the same side of the molecule (Figure 4a). In addition, ROESY

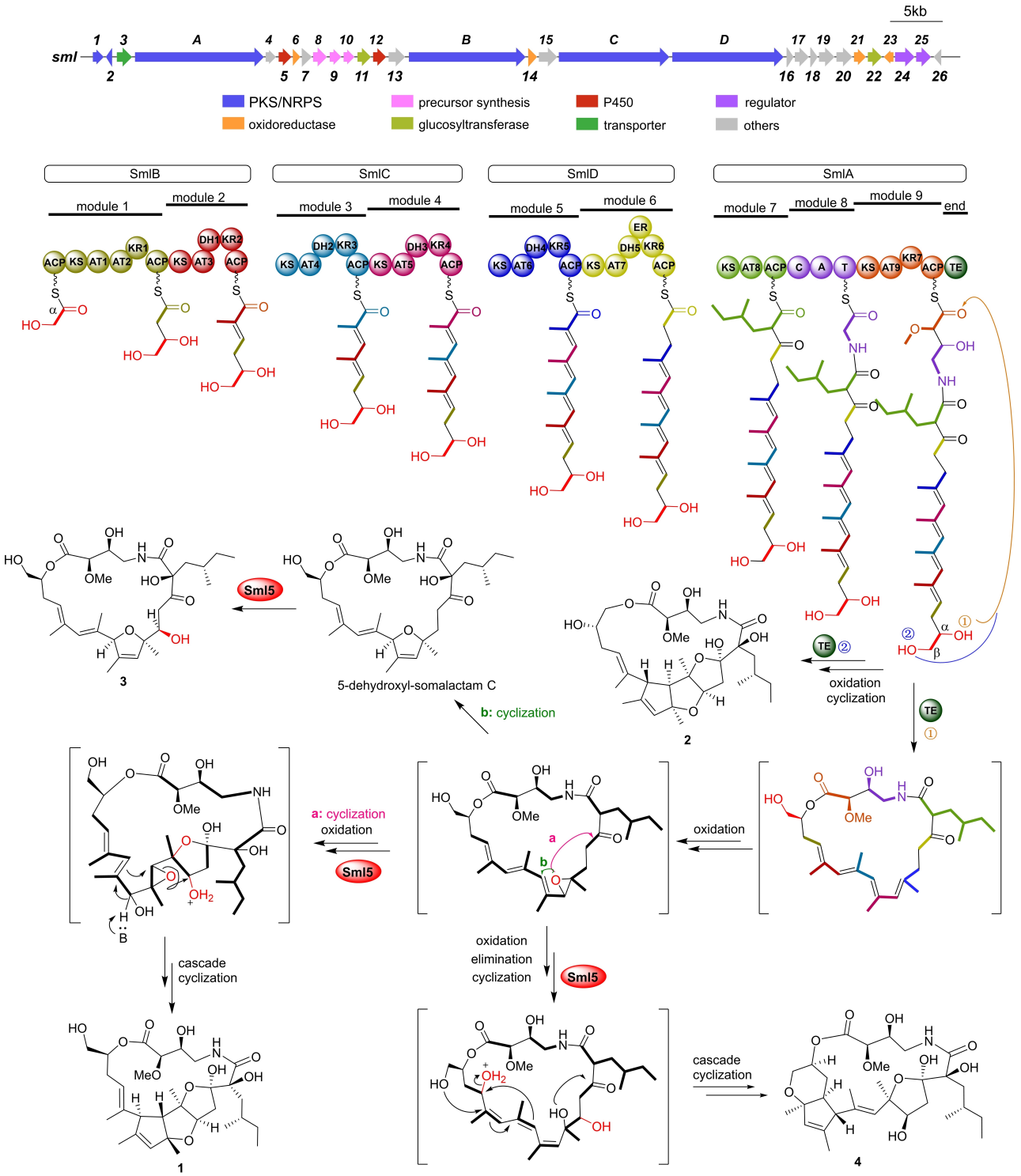

Figure 5. The biosynthetic gene cluster *sml* in *S. somaliensis* 1107 and the proposed biosynthetic route to somalactams (①, intramolecular cyclization involving α-OH; ②, intramolecular cyclization involving β-OH; a, epoxide nucleophilic cyclization; b, olefin-epoxide cyclization. Compounds in brackets are proposed intermediates).

correlations of H_3-26/H-11 and H-11/H-13 were observed, indicating that they resided on the same face. Importantly, the clear ROESY correlations of 30-OMe and H-11 revealed the stereochemical relationship between the northern and southern hemispheres of the macrocycle. A ROESY experiment involving $CDCl_3$ was conducted to consolidate the previous configurational analysis, and the correlation peak of 30-OMe/H-11 was clearly observed (Figure S30). The Mosher method was then applied to establish the absolute configuration of C18, and NMR anisotropic analysis of the

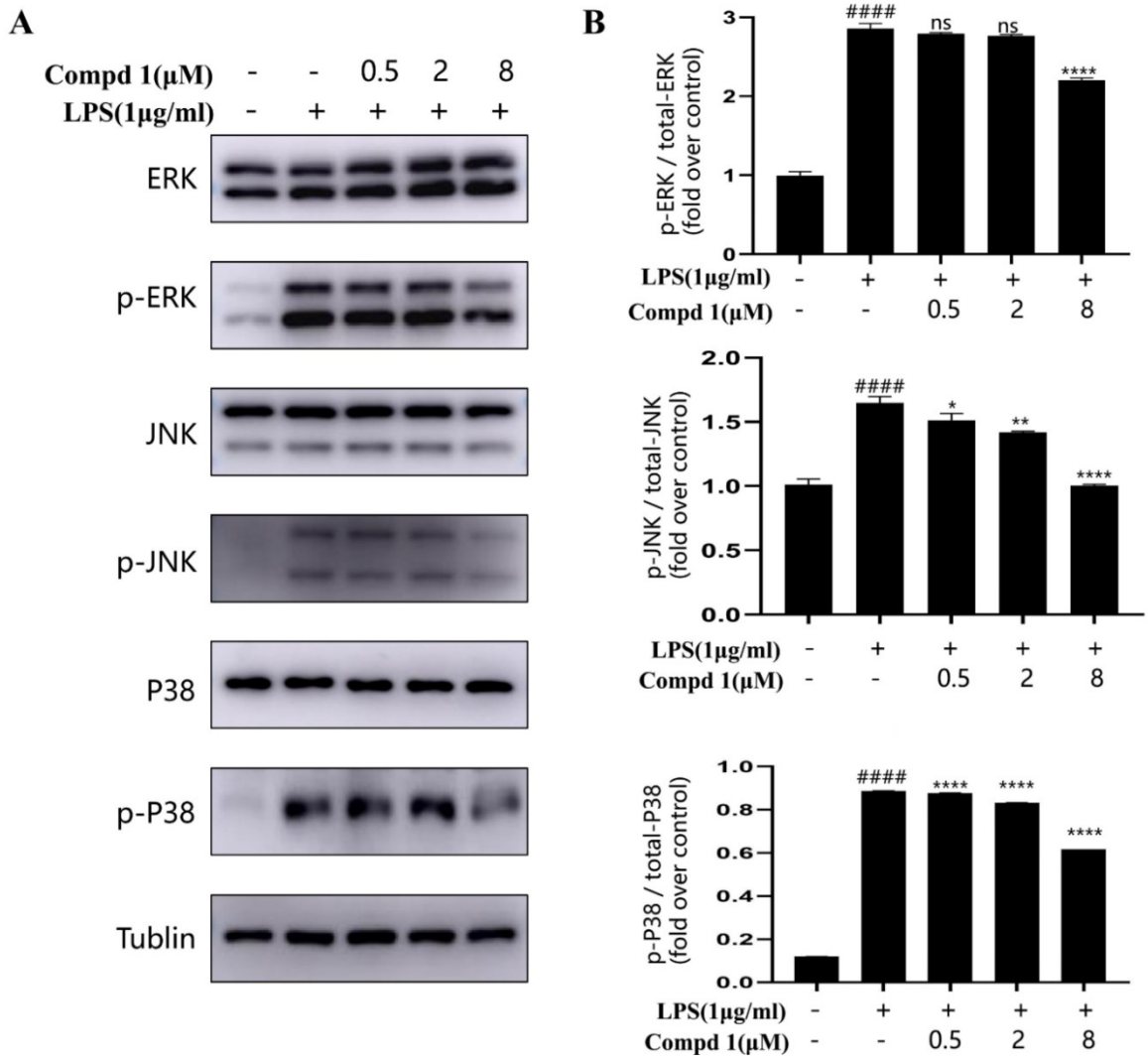

Figure 6. Effects of compound **1** on activation of LPS-induced MAPK signaling pathways. (#### $p < 0.0001$, compared with vehicle-administered group. * $p < 0.05$, ** $p < 0.01$, **** $p < 0.0001$, compared with LPS group.)

corresponding products assigned the absolute configuration of C18 as *S* (Figure S11).

The absolute configuration of **1** was determined using single-crystal X-ray diffraction analysis (Cu Kα radiation).[13] A single crystal for the X-ray diffraction was grown from a solvent system (CH_2Cl_2/MeOH/H_2O, 5:5:1) for 14 days. The result provided definitive evidence of the planar structure of **1** and also allowed the unambiguous assignment of its absolute configuration as shown (Figure 2).

Somalactam B (**2**) was isolated as a white amorphous solid. The molecular formula of **2** was assigned as $C_{30}H_{47}NO_{10}$ based on HRESIMS data, which revealed an ion peak at *m/z* 580.3136 $[M-H]^-$ ($C_{30}H_{46}NO_{10}$, calcd. 580.3122). An extensive examination of the 1D and 2D NMR data suggested that it had an almost identical planar structure to **1** except for the linkage between fragments A and B (Table S6). This difference was confirmed by the key HMBC correlations from the oxymethylene protons H_2-16 ($\delta_H = 4.14$, 3.89 ppm) to C14 ($\delta_C = 37.1$ ppm), C15 ($\delta_C =$ 68.3 ppm), and the ester carbonyl C17 ($\delta_C = 169.2$ ppm). Therefore, the planar structure of **2** was established (Figure 3). The relative configuration of **2** was determined by ROESY analysis (Figure 4b). The diagnostic ROESY correlations of H-11/H_3-26, H-5/H_3-27, H-5/H_3-26, H-11/H_3-27, and H-21a/3-OH suggested that they were oriented on the same side of the molecule. Suitable crystals of **2** for crystallographic experiments were obtained by a slow evaporation method ($MeOH/H_2O$ 2:1, −4 °C, about 10 days). Accordingly, the absolute configuration of **2** was determined by the fine Cu Kα crystallographic data (Figure 2).

Somalactam C (**3**) was obtained as a white amorphous solid. The molecular formula of **3** was established as $C_{30}H_{47}NO_{10}$ by the molecular ion peak at *m/z* 604.3107 $[M+Na]^+$ ($C_{30}H_{47}NO_{10}Na$, *calcd.* 604.3098). An extensive inspection of the 2D NMR data of **3** suggested that it had four substructural units (A–D), sharing the same A and B moieties as those in **1** (Figure S7). For fragment C (C6-C11),

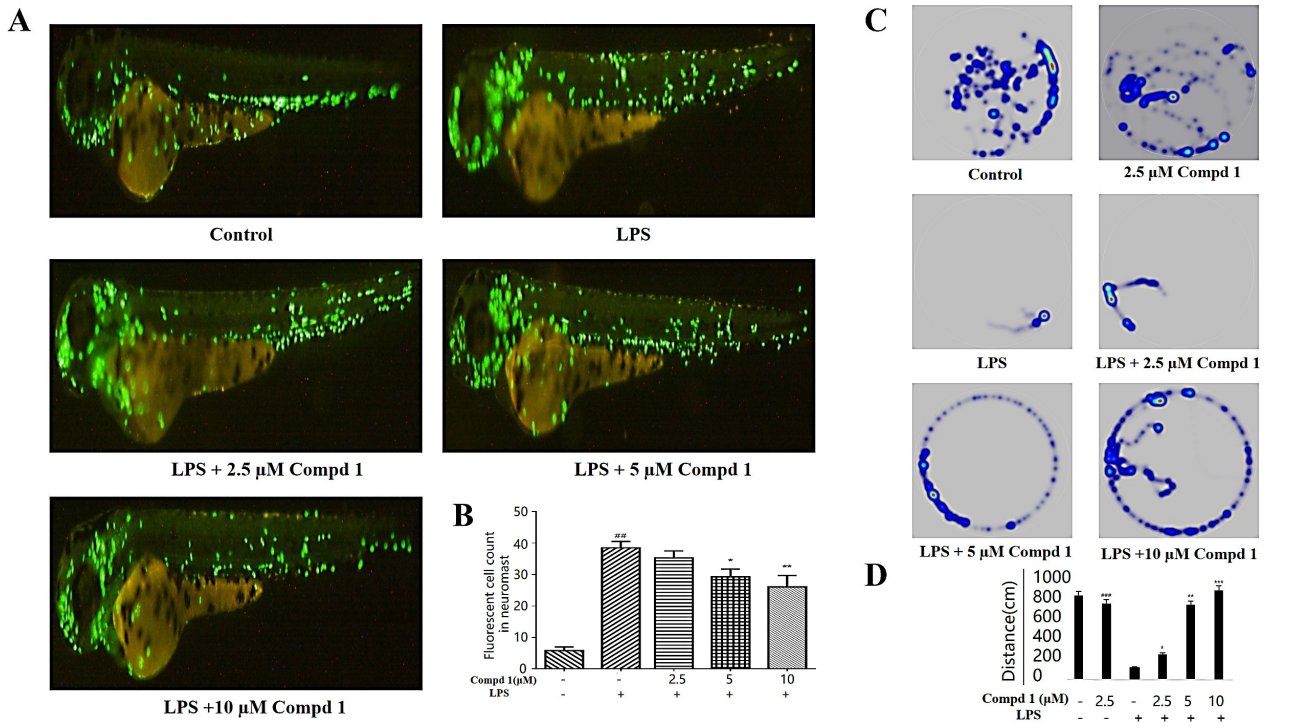

Figure 7. Anti-inflammatory activity assays. A, B) In vivo tracking of changes in GFP-labeled inflammatory cells in transgenic zebrafish treated with LPS and compound **1**. C, D) The swimming behavior of zebrafish larvae was detected after they were treated with LPS and compound **1**.

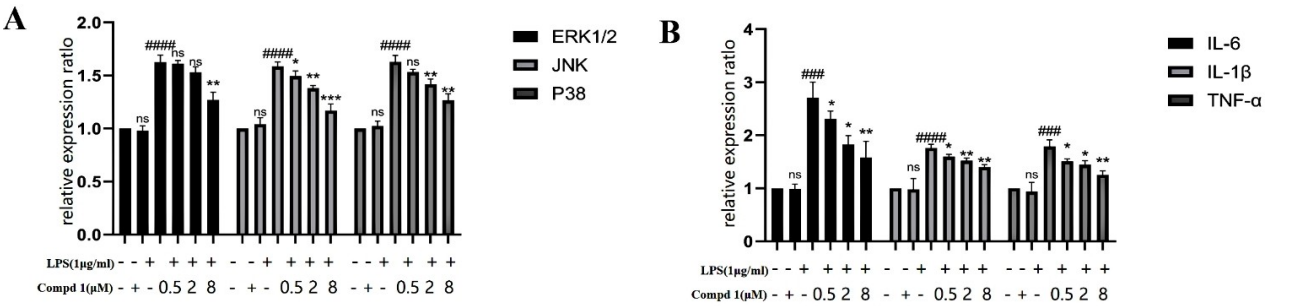

Figure 8. The mRNA expression levels of ERK1/2, JNK, p38, IL-6, IL-1β, and TNF-α upon compound **1** pretreatment. ($^{###}$ $p<0.001$, $^{####}$ $p<0.0001$, compared with vehicle-administered group. * $p<0.05$, ** $p<0.01$, *** $p<0.001$, compared with LPS group.)

the HMBC correlations from the oxymethine proton H-9 ($\delta_H=4.80$ ppm) to the olefin carbon atoms C7 and C8 and from the olefin proton H-7 ($\delta_H=5.64$ ppm) to C6 ($\delta_C=89.9$ ppm) and C9 ($\delta_C=92.2$ ppm), together with the allylic COSY correlation of H-7/H-9, indicated the presence of a 2,5-dihydrofuran ring. In fragment D (C1-C5), hydroxy and ketone groups were placed at C5 and C3, respectively, as indicated by the COSY correlations between the oxymethine proton H-5 and H_2-4 and the HMBC correlation from H-4a to C3 ($\delta_C=207.6$ ppm) and C2 ($\delta_C=83.7$ ppm). The HMBC correlations from 2-OH ($\delta_H=6.16$ ppm) and H-20b to the amide carbonyl C1 ($\delta_C=170.7$ ppm), together with those of H_3-25/C5, C6, and C7, established the linkages between fragments A and D and between fragments C and D; thus, a 21-membered macrolide lactam was determined. In the ROESY spectrum, the correlation between H-9 and H_3-25 suggested that they were on the same side. The ROESY correlations of H_3-28/H-11 and H_3-27/H-13 indicated that the double bonds of Δ^{10} and Δ^{12} were in the *E* configuration (Figure 4b). Suitable crystals of **3** for X-ray crystallographic analysis were obtained from a mixed MeOH/H_2O (3:1) solution. Therefore, the absolute configuration of **3** was unambiguously determined using single-crystal X-ray diffraction (Figure 2).

Somalactam D (**4**) was obtained as a white amorphous solid. The molecular formula, $C_{30}H_{47}NO_{10}$, was established by HRESIMS identification of a positive ion at *m/z* 604.3078 $[M+Na]^+$ ($C_{30}H_{47}NO_{10}Na$, calcd. 604.3098). Inspection of its 1D and 2D NMR data suggested that **4** was similar to **1**, with the difference being in the B moiety (C9-C15; Table S8). In fragment B, the COSY correlations of H-13/H_2-14/H-15/H_2-29 together with the HMBC correlations from H-14b to the

oxygenated carbons C12 (δ_C = 82.3 ppm), C29 (δ_C = 61.3 ppm) and C15 (δ_C = 68.3 ppm), revealed a tetrahydro-2*H*-pyran moiety. Furthermore, the COSY correlation of H-11/H_3-27 and the HMBC correlations from H_3-27 to C9, C10 and C11, from H-11 to C13, and from H-9 to C10 and C13 suggested the presence of a hexahydrocyclopenta[*b*]pyran ring system. The absolute configuration of **4** was determined by single-crystal X-ray diffraction analysis (Cu Kα radiation; Figure 2). The single crystals were obtained from a ternary solvent of CH_2Cl_2/MeOH/H_2O (5:5:1) after 8 days.

Biosynthetically, in line with typical biosynthetic mechanisms for PKS-NRPS-derived natural products,[14] we reasoned that somalactam formation begins with the condensation between a rare glycolyl-CoA unit and an ACP-bound malonyl-CoA (M-CoA) catalyzed by module 1 of SmlC. Biosynthesis then continues by elongation with four methylmalonyl-CoA units (mM-CoA), one malonyl-CoA unit, and another rare extender unit 4-methylhexanoyl-CoA followed by extension with glycine by the condesation (C) domain in module 8 of SmlA and further condensation with 4-methoxymalonyl-CoA. The mature PKS-NRPS-PKS intermediate is released from the hybrid PKS/NRPS assembly line after the formation of the macrolactone ring by the terminal TE domain (Figure 5). The order and function of domains encoded by genes *smlA* to *smlD* exactly follows the model suggested by the structure of the core macrolactone and the PKS pattern of collinearity.

Further analysis of the substrate specificities of the AT domains (Figure S8) by protein sequence alignments revealed that AT2 and AT7 are responsible for selecting M-CoA and four AT domains (AT3-AT6) specifically incorporate mM-CoA. In addition, AT9 contains the residues that have been predicted to specify the selection of the atypical extender unit methoxymalonate, as demonstrated by the biosynthesis of the macrolides bafilomycin, geldanamycin, ansamytocin, and pellasoren.[15] However, we failed to identify residues specifically related to AT1 and AT8 domain substrates through sequence alignments (Figure S8). Based on the structural characteristics of somalactams, we propose that AT1 might recognize and activate a glycolate-derived extender unit, which is rare in natural products as exemplified by amphidinol, FK-520 biosynthesis, soraphen, and ansamitocin.[16] AT8 is hypothesized to extend another rarely observed "2-methyl-butyrylmalonyl-CoA" extender unit.[17] Stable isotope feeding studies are necessary to probe the substrate specificity of the AT domains.

In plants, the biosynthetic origin of the 4-methylhexanoyl group has been shown to occur by a "one carbon per cycle" elongation mechanism mediated by ketoacyl-ACP synthase III (KASIII).[18] Interestingly, one putative KASIII encoding gene *sml9* is located in the *sml* gene cluster (Table S1). Based on the alpha-ketoacid elongation (α-KAE) reaction performed by KASIII, we propose that, after the formation of a 3-methyl-2-oxovaleryl-CoA intermediate by reactions of branched-chain amino acid metabolism, it would undergo two cycles of α-KAE catalyzed by KASIII-Sml9 to yield 4-methylhexanoyl-CoA. This is further converted into the atypical extender unit 2-methyl-butyrylmalonyl-CoA through reductive carboxylation catalyzed by the adjacent putative dehydrogenase Sml10 and crotonyl-CoA carboxylase/reductase Sml8.[19] Further experiments are underway in our laboratories to investigate the biosynthesis of the branched C7 unit.

Next, we analyzed the bioinformatic structure predictions in detail based on the distribution of the ketoreductase (KR),[20] dehydratase (DH),[21] and enoyl reductase (ER)[22] domains in the PKS modules by antiSMASH predictions and active-site sequence alignments (Figure S8). All the domains identified in the *sml* gene cluster are functional and consistent with the NMR and X-ray structures. Specifically, the KR7 domain in module 9 lacks the "LDD" motif, typically conserved in type-B KR. Thus, KR7 was assigned as a type-A1 KR, generating an $_L$-β-hydroxy group (Figure S8).[20,23] Accordingly, the absolute configuration of the corresponding hydroxy group was assigned an *S* configuration, as confirmed by NMR and X-ray analysis.

The differences between the predicted structure based on the PKS-NRPS assembly line and the isolated chemical structure can be accounted for by post-modification enzymes. There are a number of genes encoding oxidative tailoring enzymes in the *sml* gene cluster, such as P450s, FMOs, and oxidoreductases (Table S1).[24] The deletion of P450 Sml5 led to the production of three new peaks in the mass spectrum with a 16 Dalton loss. One of the three metabolites was isolated and identified as 5-dehydroxyl-somalactam C (Figure S5 and Figure S6), indicating a potential role for SmI5 in the C5 hydroxylation of the macrolide backbone.

Thus, the core scaffold derived from PKS-NRPS-PKS megasynthases was modified and rearranged by these oxidative enzymes, including the formation of the intriguing fused tricyclic ether system of **1** and **2**.[24b,25] Hypothetically, the tricyclic system of **1** could be constructed from a cationic cyclization cascade, epoxide attack of the protonated hydroxy group, and olefin cyclization onto the opened epoxide. The fused furan moiety of **4** could be constructed through Prins-type cyclization followed by O-cyclization.[26]

The anti-inflammatory activities of **1**–**4** were evaluated by measuring the production of two pro-inflammatory cytokines, namely, interleukin-6 (IL-6) and tumor necrosis factor-α (TNF-α), in the serum of lipopolysaccharide (LPS)-stimulated RAW264.7 macrophage cells using an Elisa method (see Supporting Information). Compound **1** inhibited IL-6 and TNF-α release with IC_{50} values of 5.76 and 0.18 μM, respectively; the other compounds displayed no activity. Additionally, **1** showed no cytotoxicity to 12 human cancer cell lines and the RAW264.7 cell line (IC_{50} > 100 μM); therefore, it exhibited anti-inflammatory potential.

In response to inflammatory stimuli that activate macrophages, intracellular signaling pathways are activated that carry the signals needed to activate the production of inflammatory mediators. Primary inflammatory stimuli (microbial products) and cytokines such as IL-1β and TNF-α can activate mitogen-activated protein kinase (MAPK) pathways. Moreover, the continuous activation of the MAPK signaling pathway can, in turn, promote the expression of TNF-α, IL-6, and other factors.[27] Thus, we investigated whether **1** could affect this pathway. We

examined the expression levels of phosphorylated MAPK family members (i.e., p38, ERK1/2, and JNK). Western blot analysis revealed that treatment with different concentrations of **1** significantly decreased the expression levels of phosphorylated ERK1/2, JNK, and p38 ($p < 0.05$) in LPS-induced RAW264.7 cells (Figure 6). After treatment with 8 μM compound **1** for 12 h, the protein expression levels of p-ERK1/2, p-JNK, and p-p38 greatly decreased by 25.17 %, 37.52 %, and 27.03 %, respectively, compared with the LPS group ($p < 0.05$). Therefore, **1** can inhibit the LPS-activated phosphorylation of the MAPK pathway.

We used transgenic zebrafish (Tg:zlyz-EGFP) to evaluate the effects of somalactam A (**1**) on the production of inflammatory factors and the motility of LPS-treated zebrafish. Transgenic zebrafish (Tg:zlyz-EGFP) can express enhanced green fluorescent protein (EGFP) in macrophages, and the more macrophages that produce pro-inflammatory factors, the more GFP signals detected.[28] The more intense the inflammation is, the weaker the motility of the zebrafish.[29]

LPS can induce the proliferation of macrophages, leading to systemic inflammation.[30] However, **1** could significantly inhibit the LPS-induced increase in macrophage numbers in zebrafish larvae in a dose-dependent manner. The intensity of GFP signals in the zebrafish larvae pretreated with 10 μM compound **1** and 1 $\mu g\,mL^{-1}$ LPS was significantly decreased by 18.80 % compared with that in the zebrafish larvae treated with LPS alone ($p < 0.05$, Figure 7A,B). Figure 7C,D shows that LPS treatment markedly altered the swimming behavior and reduced the total swimming distance of zebrafish larvae by 10.92-fold as compared with those in the control group; pretreatment with **1** reduced this deficit in a dose-dependent manner. Moreover, 10 μM compound **1** improved the total movement distance by 11.59-fold as compared with that in the LPS-alone treatment group, indicating that **1** protected against LPS-induced movement defects.[31] Further, there was no significant change in swimming distance in the zebrafish group with **1** alone compared to the control group. Additionally, the effects of **1** on the expression levels of key proteins of the MAPK pathway and genes downstream of proinflammatory cytokines in LPS-induced zebrafish larvae were evaluated using RT-qPCR. The LPS treatment significantly increased the mRNA expression levels of ERK1/2, JNK, p38, IL-6, TNF-α, and IL-1β ($p < 0.05$, Figure 8), while the expression levels of ERK1/2, JNK, p38, IL-6, TNF-α, and IL-1β significantly decreased ($p < 0.05$) in compound **1**-pretreated LPS-induced zebrafish, which is consistent with the results from in vitro experiments (Figure 8). For example, pretreatment with 10 μM compound **1** decreased the IL-6, TNF-α, and IL-1β expression levels by 65.75 %, 56.04 %, and 57.95 %, respectively, compared with those in the LPS-alone treatment group.

Conclusion

In summary, somalactams, a novel group of macrolide lactams with unique ring systems, were isolated from the Arctic sponge associated actinomycete *S. somaliensis* 1107. The structures of the somalactams were elucidated through the integrated interpretation of HRESIMS data, NMR spectra, and single-crystal X-ray diffraction. The biosynthetic mechanism proposed herein provides insight into the enzymatic machinery of macrolide lactams and also a hint for discovery of novel natural products from marine-derived microorganisms. The potent anti-inflammatory activity without cytotoxicity of this rare macrolide lactam renders **1** a promising candidate for drug discovery and development, deserving of further investigation.

Acknowledgements

This research was funded by the National Key Research and Development Program of China (2022YFC2804300, 2022YFC2804100), the National Natural Science Foundation of China (U2106227, 82022066, 82073758 and22137006), the Taishan Scholar Project from Shandong Province (ts20190950), the Shandong Provincial Natural Science Foundation (ZR2021ZD28), the Shenzhen Fundamental Research Program (20220523121619003), the Oceanic Interdisciplinary Program of Shanghai Jiao Tong University (SL2020MS029), the Open Project of National Major Science and Technology Infrastructure of Translational Medicine (TMSK-2021-206), and the Open Projects Fund of SKLMT of Shandong University (M2021-04). The authors thank Yuan Tian, Jing He, and Dr. Wei-Zhuo Tang for providing assistance for experiments and manuscript writing. We also thank Zhifeng Li, Jingyao Qu, and Jing Zhu of the Core Facilities for Life and Environmental Sciences, State Key laboratory of Microbial Technology of Shandong University for HR-LCMS analysis.

Conflict of Interest

The authors declare no conflict of interest.

Data Availability Statement

The data that support the findings of this study are available in the supplementary material of this article.

Keywords: Anti-Inflammatory Activity · Biosynthesis · Macrolide Lactams · Marine Natural Products · Structure Elucidation

[1] a) Z. E. Wilson, M. A. Brimble, *Nat. Prod. Rep.* **2009**, *26*, 44–71; b) S. Soldatou, B. J. Baker, *Nat. Prod. Rep.* **2017**, *34*, 585–626; c) P. Nopnakorn, P. Nopnakorn, *J. Nat. Sci. Res.* **2018**, *8*, 30–43; d) V. C. Tripathi, S. Satish, S. Horam, S. Raj, A. lal, J. Arockiaraj, M. Pasupuleti, D. K. Dikshit, *Polar Sci.* **2018**, *18*, 147–166; e) L. J. Silva, E. J. Crevelin, D. T. Souza, G. V. Lacerda-Júnior, V. M. de Oliveira, A. L. T. G. Ruiz, L. H. Rosa, L. A. B. Moraes, I. S. Melo, *Sci. Rep.* **2020**, *10*, 13870.

[2] V. R. Macherla, J. Liu, C. Bellows, S. Teisan, B. Nicholson, K. S. Lam, B. C. Potts, *J. Nat. Prod.* **2005**, *68*, 780–783.
[3] W. Zhang, Z. Liu, S. Li, T. Yang, Q. Zhang, L. Ma, X. Tian, H. Zhang, C. Huang, S. Zhang, J. Ju, Y. Shen, C. Zhang, *Org. Lett.* **2012**, *14*, 3364–3367.
[4] a) W. Liu, W. Zhang, H. Jin, Q. Zhang, Y. Chen, X. Jiang, G. Zhang, L. Zhang, W. Zhang, Z. She, C. Zhang, *Mar. Drugs* **2019**, *17*, 663; b) R. Raju, A. M. Piggott, M. M. Conte, R. J. Capon, *Org. Biomol. Chem.* **2010**, *8*, 4682–4689.
[5] C. Hohmann, K. Schneider, C. Bruntner, E. Irran, G. Nicholson, A. T. Bull, A. L. Jones, R. Brown, J. E. Stach, M. Goodfellow, W. Beil, M. Krämer, J. F. Imhoff, R. D. Süssmuth, H. P. Fiedler, *J. Antibiot (Tokyo).* **2009**, *62*, 99–104.
[6] Y. H. Gui, L. Liu, W. Wu, Y. Zhang, Z. L. Jia, Y. P. Shi, H. T. Kong, K. C. Liu, W. H. Jiao, H. W. Lin, *Bioorg. Chem.* **2020**, *94*, 103435.
[7] K. Blin, S. Shaw, K. Steinke, R. Villebro, N. Ziemert, S. Y. Lee, M. H. Medema, T. Weber, *Nucleic Acids Res.* **2019**, *47*, W81–W87.
[8] a) F. Liu, S. Garneau, C. T. Walsh, *Chem. Biol.* **2004**, *11*, 1533–1542; b) S. Donadio, M. J. Staver, J. B. McAlpine, S. J. Swanson, L. Katz, *Science* **1991**, *252*, 675–679.
[9] a) J. Piel, *Nat. Prod. Rep.* **2010**, *27*, 996–1047; b) S. Kosol, M. Jenner, J. R. Lewandowski, G. L. Challis, *Nat. Prod. Rep.* **2018**, *35*, 1097–1109; c) H. Chen, Z. Bian, V. Ravichandran, R. Li, Y. Sun, L. Huo, J. Fu, X. Bian, L. Xia, Q. Tu, Y. Zhang, *Crit. Rev. Microbiol.* **2019**, *45*, 162–181.
[10] a) S. Romano, S. A. Jackson, S. Patry, A. D. W. Dobson, *Mar. Drugs* **2018**, *16*, 244; b) R. Pan, X. Bai, J. Chen, H. Zhang, H. Wang, *Front. Microbiol.* **2019**, *10*, 294.
[11] H. Huang, G. Zheng, W. Jiang, H. Hu, Y. Lu, *Acta. Biochim. Biophys. Sin (Shanghai).* **2015**, *47*, 231–243.
[12] N. Matsumori, D. Kaneno, M. Murata, H. Nakamura, K. Tachibana, *J. Org. Chem.* **1999**, *64*, 866–876.
[13] Deposition numbers 2164089 (compound **1**), 2164090 (compound **2**), 2164091 (compound **3**), 2164092 (compound **4**) contain the supplementary crystallographic data for this paper. These data are provided free of charge by the joint Cambridge Crystallographic Data Centre and Fachinformationszentrum Karlsruhe Access Structures service.
[14] C. T. Walsh, *Science* **2004**, *303*, 1805–1810.
[15] a) S. F. Haydock, J. F. Aparicio, I. Molnár, T. Schwecke, L. E. Khaw, A. König, A. F. Marsden, I. S. Galloway, J. Staunton, P. F. Leadlay, *FEBS Lett.* **1995**, *374*, 246–248; b) C. Jahns, T. Hoffmann, S. Müller, K. Gerth, P. Washausen, G. Höfle, H. Reichenbach, M. Kalesse, R. Müller, *Angew. Chem. Int. Ed.* **2012**, *51*, 5239–5243; *Angew. Chem.* **2012**, *124*, 5330–5334; c) W. Zhang, J. L. Fortman, J. C. Carlson, J. Yan, Y. Liu, F. Bai, W. Guan, J. Jia, T. Matainaho, D. H. Sherman, S. Li, *ChemBioChem* **2013**, *14*, 301–306; d) L. Ray, B. S. Moore, *Nat. Prod. Rep.* **2016**, *33*, 150–161.
[16] a) A. Cutignano, G. Nuzzo, A. Sardo, A. Fontana, *Mar. Drugs* **2017**, *15*, 157; b) J. N. Andexer, S. G. Kendrew, M. Nur-e-Alam, O. Lazos, T. A. Foster, A. S. Zimmermann, T. D. Warneck, D. Suthar, N. J. Coates, F. E. Koehn, J. S. Skotnicki, G. T. Carter, M. A. Gregory, C. J. Martin, S. J. Moss, P. F. Leadlay, B. Wilkinson, *Proc. Natl. Acad. Sci. USA* **2011**, *108*, 4776–4781; c) S. C. Wenzel, R. M. Williamson, C. Grünanger, J. Xu, K. Gerth, R. A. Martinez, S. J. Moss, B. J. Carroll, S. Grond, C. J. Unkefer, R. Müller, H. G. Floss, *J. Am. Chem. Soc.* **2006**, *128*, 14325–14336.
[17] M. C. Wilson, B. S. Moore, *Nat. Prod. Rep.* **2012**, *29*, 72–86.
[18] a) L. Kandra, G. J. Wagner, *Phytochemistry* **1998**, *49*, 1599–1604; b) N. Sugimoto, P. Engelgau, A. D. Jones, J. Song, R. Beaudry, *Proc. Natl. Acad. Sci. USA* **2021**, *118*, e2009988118.
[19] a) C. Y. Lai, J. E. Cronan, *J. Biol. Chem.* **2003**, *278*, 51494–51503; b) R. Nofiani, B. Philmus, Y. Nindita, T. Mahmud, *MedChemComm* **2019**, *10*, 1517–1530; c) T. Miyazawa, S. Takahashi, A. Kawata, S. Panthee, T. Hayashi, T. Shimizu, T. Nogawa, H. Osada, *J. Biol. Chem.* **2015**, *290*, 26994–27011; d) L. Yang, F. Ye, J. Liu, D. J. Klionsky, D. Tang, R. Kang, *Autophagy* **2022**, 1–12.
[20] A. Baerga-Ortiz, B. Popovic, A. P. Siskos, H. M. O'Hare, D. Spiteller, M. G. Williams, N. Campillo, J. B. Spencer, P. F. Leadlay, *Chem. Biol.* **2006**, *13*, 277–285.
[21] D. L. Akey, J. R. Razelun, J. Tehranisa, D. H. Sherman, W. H. Gerwick, J. L. Smith, *Structure* **2010**, *18*, 94–105.
[22] D. H. Kwan, Y. Sun, F. Schulz, H. Hong, B. Popovic, J. C. Sim-Stark, S. F. Haydock, P. F. Leadlay, *Chem. Biol.* **2008**, *15*, 1231–1240.
[23] M. C. Kim, H. Machado, K. H. Jang, L. Trzoss, P. R. Jensen, W. Fenical, *J. Am. Chem. Soc.* **2018**, *140*, 10775–10784.
[24] a) P. Durairaj, S. Li, *Eng. Microbiol.* **2022**, *2*, 100011; b) Z. Li, Y. Jiang, F. P. Guengerich, L. Ma, S. Li, W. Zhang, *J. Biol. Chem.* **2020**, *295*, 833–849; c) W. Zhang, L. Du, F. Li, X. Zhang, Z. Qu, L. Han, Z. Li, J. Sun, F. Qi, Q. Yao, Y. Sun, C. Geng, S. Li, *ACS Catal.* **2018**, *8*, 9992–10003.
[25] a) J. Amiri Moghaddam, T. Jautzus, M. Alanjary, C. Beemelmanns, *Org. Biomol. Chem.* **2021**, *19*, 123–140; b) X. Zhang, S. Li, *Nat. Prod. Rep.* **2017**, *34*, 1061–1089.
[26] X. Han, G. Peh, P. E. Floreancig, *Eur. J. Org. Chem.* **2013**, 1193–1208.
[27] a) D. M. González Mosquera, Y. Hernández Ortega, P. L. Fernández, Y. González, D. Doens, Y. Vander Heyden, K. Foubert, L. Pieters, *Phytother. Res.* **2018**, *32*, 1750–1754; b) C. Xie, J. Kang, Z. Li, A. G. Schauss, T. M. Badger, S. Nagarajan, T. Wu, X. Wu, *J. Nutr. Biochem.* **2012**, *23*, 1184–1191.
[28] a) B. Ye, X. Xiong, X. Deng, L. Gu, Q. Wang, Z. Zeng, X. Gao, Q. Gao, Y. Wang, *Pharm. Biol.* **2017**, *55*, 673–679; b) Y. H. Gui, W. H. Jiao, M. Zhou, Y. Zhang, D. Q. Zeng, H. R. Zhu, K. C. Liu, F. Sun, H. F. Chen, H. W. Lin, *Org. Lett.* **2019**, *21*, 767–770.
[29] a) V. L. L. Lee, A. Norazit, S. M. Noor, M. F. Shaikh, *Front. Pharmacol.* **2022**, *13*, 821618; b) B. K. Park, N. S. Kim, Y. R. Kim, C. Yang, I. C. Jung, I. S. Jang, C. S. Seo, J. J. Choi, M. Y. Lee, *Front. Pharmacol.* **2020**, *11*, 958.
[30] a) R. Zanandrea, C. D. Bonan, M. M. Campos, *Drug Discovery Today* **2020**, *25*, 2201–2211; b) M. C. Gomes, S. Mostowy, *Trends Microbiol.* **2020**, *28*, 10–18.
[31] W. Wu, H. Han, J. Liu, M. Tang, X. Wu, X. Cao, T. Zhao, Y. Lu, T. Niu, J. Chen, H. Chen, *Oxid. Med. Cell. Longevity* **2021**, *2021*, 6688708.

Manuscript received: December 7, 2022
Accepted manuscript online: January 21, 2023
Version of record online: March 24, 2023